# Dalton Transactions

Accepted Manuscript






ROYAL SOCIETY OF CHEMISTRY

www.rsc.org/dalton

Journal Name

ARTICLE

# A Doubly Deprotonated Diimine Dioximate Metalloligand as a Synthon for Multimetallic Complex Assembly

Received 00th January 20xx,
Accepted 00th January 20xx

DOI: 10.1039/x0xx00000x

www.rsc.org/

Danielle A. Henckel,[a] Yuting F. Lin,[a] Theresa M. McCormick,[b] Werner Kaminsky,[a] and Brandi M. Cossairt[a]*

An electrocatalytically active cobalt diimine monoxime monoximate complex was deprotonated by 1-methylimidazole affording a doubly deprotonated complex that serves as a versatile precursor for synthesis of a variety of multimetallic complexes with Co–Zn, –Cd, –Mn and –Ru coordination. These complexes were studied using a combination of spectroscopic, analytical and electrochemical techniques, revealing the electronic and structural parameters unique to this new class of compounds. The ability of these complexes to catalyze proton reduction was also investigated. These complexes are homogeneous electrocatalysts for the hydrogen evolution reaction through reduction of $[NEt_3H][BPh_4]$ in $CH_3CN$, however decompose under extended electrolysis conditions.

## Introduction

The investigation of bimetallic complexes for catalytic applications has been driven by the ability of a second metal center to tune the properties of the primary catalyst.[1-4] The synthesis of bimetallic complexes, however, can be challenging owing to difficulties in ligand synthesis and site-specific metallation. A versatile monometallic precursor for the synthesis of bimetallic complexes would be useful in the synthesis and subsequent studies of the effects of the bimetallic motif on the reactivity of the resulting complexes. Further, an intriguing class of photoactive catalysts where a chromophoric (light-absorbing) center is directly attached to a catalytic site could be accessed through this approach.

A diverse family of metal diimine monoxime monoximate[5-7] and diglyoxime[8-15] complexes have been studied for use as proton reduction catalysts. The synthesis of bimetallic diimine monoxime monoximate complexes has been previously explored through *in situ* deprotonation of the oxime proton.[16-19] This strategy has provided access to a variety of bimetallic complexes; however this strategy is not broadly generalizable.

We became interested in the idea of preparing an isolable, doubly deprotonated diimine dioximate complex to serve as a versatile ligand for the construction of multimetallic catalysts. Reports on the structure of a parent diimine monoxime monoximate cobalt complex containing an ethylene backbone have shown a long O-O interatomic distance, suggesting that no hydrogen bond exists between the two *cis*-oxime oxygen atoms.[20] We have found that this proton is removed by addition of an imidazole base and the resulting *cis* doubly deprotonated dioximate species can be easily isolated. The versatility of this *cis* doubly deprotonated dioximate metalloligand can be seen in its ability to bind a range of cations, including $H^+$, $Zn^{2+}$, $Cd^{2+}$, $Mn^{2+}$, and $Ru^{2+}$ with a variety of ancillary ligands, making this approach generalizable to the synthesis of multimetallic complexes.

## Results and Discussion

The doubly deprotonated cobalt(III) diimine dioximate cation ligated by two axial 1-methylimidazole groups, $[(DO)_2en(Im^{Me})_2Co]^+$ complex **1**, is synthesized as the perchlorate salt by addition of excess 1-methylimidazole and one equivalent of zinc perchlorate to the cobalt(III) diimine monooxime monooximate starting material, $(DO)(DOH)enCoBr_2$, in $CH_3CN$ (Scheme 1). After stirring overnight, a golden solid precipitates out of the red-brown solution. The choice of zinc perchlorate is advantageous since the resulting zinc bromide and any zinc containing byproducts are very soluble in $CH_3CN$ allowing for clean precipitation of **1** from solution. Complex **1** can be isolated using other counter anions, however care must be taken to avoid the use of unsequestered alkali metal salts for the anion exchange, as sodium binds readily in the O-O binding pocket. This is evidenced by our isolation of $[(DO)_2en(Im^{Me})_2CoNa][PF_6]_2$ and $[(DO)_2en(Im^{Me})_2CoNa\text{-}15crown5][BPh_4]_2$ (Figure S1).

**Scheme 1.** Synthesis of $[(DO)_2en(Im^{Me})_2Co]^+$ (**1**)

[a] University of Washington, Department of Chemistry, Box 351700, Seattle, WA 98195-1700.
[b] Portland State University, Department of Chemistry, Box 751, Portland, OR 97207.
* Corresponding author: cossairt@chem.washington.edu
Electronic Supplementary Information (ESI) available: Additional data including NMR spectra, DFT calculation details and additional electrochemical data and analysis can be found in the Supplementary Information document. See DOI: 10.1039/x0xx00000x

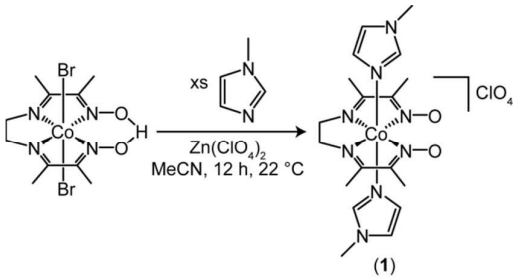


(**1**)

Addition of zinc dibromide to **1** in methanol affords bimetallic $(DO)_2en(Im^{Me})_2CoZnBr_2$ (**2**) after stirring overnight (Scheme 2a). Utilizing water as a solvent or co-solvent in this synthesis affords the tetrametallic species $[((DO)_2en(Im^{Me})_2Co)_3Zn]^{5+}$ (**3-Zn**, Scheme 2b). Therefore, the stoichiometry in the CoZn system can be controlled by solvent choice. We have synthesized and characterized the tetrametallic species **3-M**, M= Zn, Cd, Mn, from their corresponding perchlorate salts in 1:1 water/methanol with three equivalents of **1**. We observed that the $^1$H NMR spectra of complexes **2** and **3-Zn** are concentration dependent in DMSO-$d_6$, with the resonances approaching that of complex **1** at concentrations below 0.4 mM. This is corroborated by the crystallization of $[((DO)_2en(Im^{Me})_2Co)_2Zn(HOMe)]^{4+}$ under these conditions (Figure S2). In less polar solvents, such as $CD_3CN$, the $^1$H NMR resonances are independent of concentration and UV-vis spectra show distinct peaks in $CH_3CN$ (*vide infra*). In order to elucidate whether the binding of zinc dibromide is an equilibrium process in $CH_3CN$, titration of zinc dibromide into complex **1** was monitored by UV-vis spectroscopy and cyclic voltammetry (Figure S3-5). It was determined that the binding of zinc dibromide to complex **1** to form complex **2** is not an equilibrium process in $CH_3CN$, with complete conversion to **2** after addition of one equivalent of zinc dibromide.

Attempts to synthesize the bimetallic manganese and cadmium complexes from their bromide salts were unsuccessful, leading to isolation of solely complexes **3-Mn** and **3-Cd** and excess $MBr_2$. To this end, we sought an alternate way to access bimetallic species using **1**. We hypothesized that utilizing more strongly complexed starting materials with two *cis* open coordination sites, as in the case of $[Ru(bpy)_2(H_2O)_2]^{2+}$, would lead to facile formation of bimetallic complexes. Upon addition of complex **1** to $Ru(bpy)_2(H_2O)_2(OTf)_2$, in 2:1 ethanol/water overnight at 60 °C, $[(DO)_2en(Im^{Me})_2Co)Ru(bpy)_2]^{3+}$ (**4**) crystallizes cleanly after addition of excess LiOTf (Scheme 2c).

In order to make structural and spectral comparisons to **1**, as well as to perform $pK_a$ studies, $[(DOH)(DO)en(Im^{Me})_2Co)]^{2+}$, complex **1-H$^+$**, was independently synthesized from **1** by addition of [HDMF][OTf] in $CH_3CN$ and subsequent crystallization from water with excess $NaPF_6$. Exchange of the bridging proton between complex **1** and **1-H$^+$** was observed on the $^1$H NMR time scale. When a mixture of complex **1** and **1-H$^+$** is in solution in $CD_3CN$ the NMR resonances observed are mole-weighted fractions of the two components. Utilizing $^1$H NMR, a titration was performed with a protonated phosphazene ($[2\text{-}NO_2\text{-}4\text{-}CF_3\text{-}C_6H_3PH(pyrr)][PF_6]$, $pK_a$=16.54),[21] giving a $pK_a$ of 14.9 for **1-H$^+$** (Figure S6). The doubly protonated complex, with both oxime oxygens protonated, can be observed following addition of two equivalents of [HDMF][OTf]. This species was identified by UV-vis spectroscopy, which lacks any intense absorbance features in the visible, in contrast to complexes **1** and **1-H$^+$**. An estimated $pK_a$ of complex **1-H$^+$** and the doubly protonated complex were measured by titration of **1** with HCl in water, giving $pK_a$ values of ~6.5 and 2.3-2.5 respectively (Figure S7 and 8).

**Scheme 2.** Synthesis of bimetallic and tetrametallic complexes

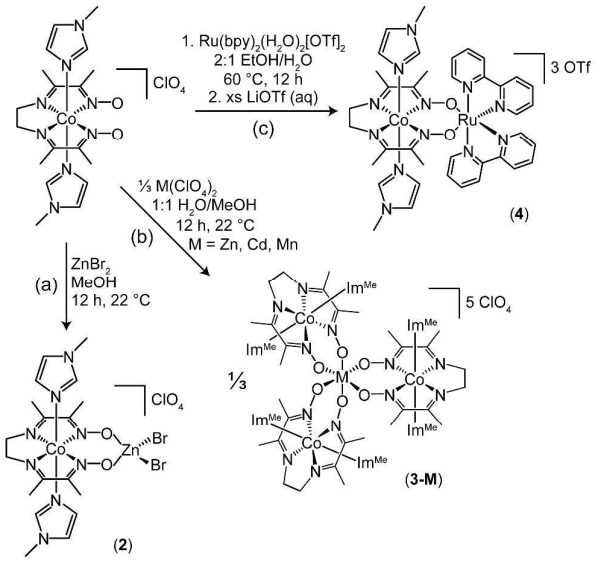


Complexes **1, 1-H$^+$, 2, 3-M** (M= Mn, Cd, Zn), and **4** were all characterized by single crystal X-ray diffraction (Figure 1a-e).[22] From the solid-state structures, the O-O interatomic distance gives further evidence for the lack of a bridging proton in **1** (3.128(4) Å vs 2.564(1) Å in **1-H$^+$**). A demonstration of the flexibility of **1** as a metalloligand is provided by the O-O interatomic distances from the crystal structures, with this distance varying by almost 0.7 Å among the complexes studied here (see Table S1). In the bimetallic species, the O-O interatomic distance lengthens to accommodate the coordinated Zn and Ru with distances of 3.197(3) and 3.24(1) Å, respectively, with the latter the largest O-O interatomic distance observed in this study. This compares to the smaller O-O interatomic distance of 3.122 Å for a similar CoMg complex previously studied using the same ethylene bridged diimine dioximate ligand framework on cobalt.[18] The O-O interatomic distances of the tetrametallic complexes correlate well with their atomic radii, in the order Cd>Mn>Zn with distances of 3.203(4), 3.071(3) and 3.061(4) Å respectively.

The UV-vis absorption spectra of **1, 1-H$^+$, 2** and **4** in $CH_3CN$ are shown in Figure 2. The transitions were assigned using time-dependent density functional theory calculations from the optimized ground state geometries using the B3LYP level of theory with LAND2Z basis set for the Ru and 6-311+G(d) for all other atoms in the Gaussian 09 suite of programs.

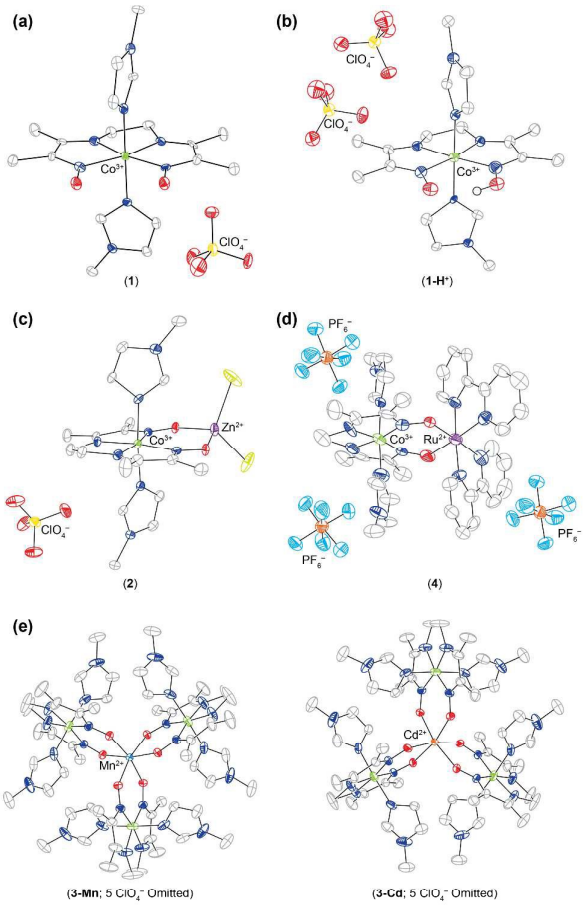


**Figure 1.** Single crystal X-ray diffraction structures of complexes **1** (a), **1-H**$^+$ (b), **2** (c), **4** (d), and **3-M** (M = Mn, Cd; e). Hydrogen atoms are omitted for clarity in (a-e) and $ClO_4$ anions are omitted for clarity in (e).

Comparison of the calculated spectra with the experimental data showed good agreement (Figure S9). Complex **1** exhibits major absorbance bands in the UV-vis region at 263, 300, 408 and 468 nm. This spectrum is dominated in the visible by the band at 408 nm, which is assigned as predominately interligand and MLCT transitions. Upon protonation to complex **1-H**$^+$, the spectral intensity decreases, but peak positions remain relatively unchanged, leading to lower extinction coefficients across all wavelengths. The UV-vis spectrum of **2** is distinct from **1** even at concentrations as low as 1.0 x$10^{-5}$ M in $CH_3CN$. Complex **2** exhibits major bands at 292 and 397 nm. The notable difference in the electronic spectra of **2** as compared to **1** is attributed to significant bromide character of the HOMO. The band at 397 nm is a result of interligand transitions. The electronic spectrum of **4** is dominated by transitions at 295, 373, 420 and 502 nm. The major absorption peak in the visible at 502 nm corresponds to MLCT transitions from d-orbitals on ruthenium to orbitals of π character on the diimine dioximate metalloligand. The second major absorption peak at 373 nm corresponds to MLCT transitions from ruthenium to bipyridine π* orbitals. No emission was observed at room temperature for complex **4**.

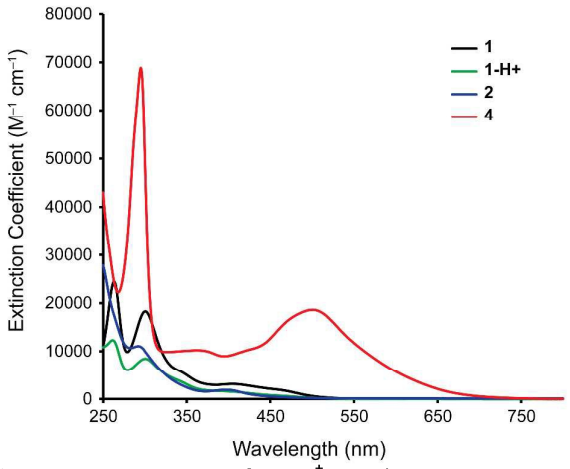


**Figure 2.** UV-Vis spectra of **1**, **1-H**$^+$, **2** and **4** in $CH_3CN$.

The cyclic voltammograms of **1**, **1-H**$^+$, **2** and **4** are shown in Figure 3 in 0.2 M [$^n$Bu$_4$N][$PF_6$] in $CH_3CN$. In **1**, the Co(III/II) and Co(II/I) couples are irreversible with reductions occurring at −1.46 and −1.69 vs $Fc^{+/0}$, respectively. Formation of a solvento species is observed following the first scan due to equilibrium binding of the $Im^{Me}$ ligands with the solvent in an apparent ECE mechanism (Figure S10).[8, 23] Electrochemical analysis of **1-H**$^+$ and **2** in $CH_3CN$ show the Co(III/II) and Co(II/I) redox events overlap to form a peak with an $E_{½}$ at -0.97 and -1.11 V vs $Fc^{+/0}$, respectively. The large $\Delta E_p$ of 82 and 94 mV for complexes **1-H**$^+$ and **2** at a scan rate of 300 mV/s suggests these are overlapping one electron waves. Titration of **1** with $ZnBr_2$ to monitor the formation of **2** by CV demonstrates that addition of 0.5 equiv $ZnBr_2$ to **1** shifts the Co(III/II) and the Co(II/I) couples anodically. Upon addition of 1.0 equiv $ZnBr_2$, the two waves coalesce on the first scan at scan rates above 10 mV/s (Figure S4). Coulometry was performed to confirm that the Co(III/II) and Co(II/I) redox events are overlapping for Complexes **1-H**$^+$ and **2** (Figure S11). After a 1 hour bulk electrolysis experiment at -1.51 V vs $Fc^{+/0}$ with complex **2,** the amount of charge passed corresponds to 2.1 $e^-$ per mole of complex. Following the first complete scan of **2** at 300 mV/s, a new reductive peak appears at -0.78 V, analogous to the solvento species observed for complex **1** (Figure S10).[24] The cyclic voltammograms of **3-M** show resolved Co(III/II) and Co(II/I) redox couples, similar to CV titrations taken of **1** with 0.5 equivalents of $ZnBr_2$ with currents that are approximately three times larger than the parent complex **1** (Figure S13). The $E_{1/2}$ of Co(III/II) and Co(II/I) are -1.06 and -1.17 V for **3-Zn**. Scanning past these potentials reveal quasi-reversible reductions (Figure S14), that are assigned as reduction to Co(0). The cyclic voltammogram of the cobalt-ruthenium complex **4** is well resolved with distinct couples for the Ru(III)/(II), Co(III)/(II), Co(II)/(I), Co(I)/(0) and two bpy/bpy(•−) couples observed in $CH_3CN$ (Figure 3). The larger difference in Co(III/II) and Co(II/I) peak separation for complex **4** may be attributed to the increased structural rigidity of this complex, as well as the close proximity of the redox active $Ru^{2+}$ metal center. Electron transfer appears to be diffusion-controlled for

all complexes since the cathodic and anodic currents vary linearly with the square root of the scan rate (Figure S15-18).[25]

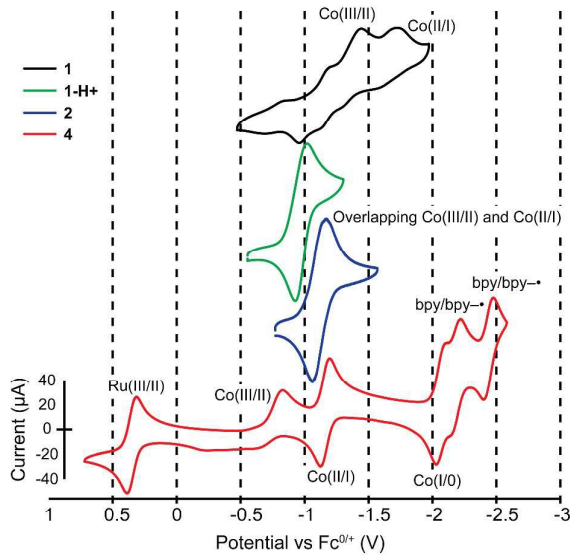


**Figure 3**. Cyclic voltammograms for **1**, **1-H$^+$**, **2** and **4**. Conditions: 0.2 M [$^n$Bu$_4$N][PF$_6$] in CH$_3$CN at 300 mV/s scan rate and 1.5 mM catalyst.

To probe the catalytic response of **1**, **1-H$^+$**, **2** and **4** to proton reduction, these complexes were treated with increasing equivalents of acid and subjected to reducing conditions by cyclic voltammetry. We have found that in electrochemical experiments using acids such as [HDMF][OTf] (pk$_a$=6.1)[26] and CF$_3$COOH (pK$_a$=12.65)[27] with Complex **1** resulted in a catalytically-active film forming on the electrode surface.[28] This was monitored using the rinse test (Figure S19).[29] The acid stability of Complex **1** was examined using $^1$H NMR spectroscopy with no decomposition products appearing following addition of 60 equiv. CF$_3$COOH under non-reducing conditions (Figure S20). Experiments utilizing a weaker acid, such as [NEt$_3$H][Cl] (pK$_a$=18.82)[21], resulted in a catalytic current response that is attributable to homogenous proton reduction catalysis yielding H$_2$, however chloride binding was found to deactivate the catalyst, leading to a cathodic drift of the catalytic response (Figure S21).[11] To avoid this, [NEt$_3$H][BPh$_4$], was used and this resulted in catalytic current that was distinct from the background glassy carbon catalytic current (Figure 4 and Figure S21-25). The homogeneous nature of the catalyst using [NEt$_3$H][BPh$_4$] as the acid source is supported by the rinse test and by evidence of a return oxidative molecular peak as seen in Figure 4b.

In most cobaloxime systems, the catalytically active species is presumed to be Co(I), which is protonated to give the Co(III)-H.[30-31] For all of our catalysts the catalytic wave begins beyond the Co(II/I) couple, suggesting that reduction of the putative Co(III)-H may be required for catalysis in our system. This is further supported by the fact that the Co(II/I) couple is more positive than the standard potential for the HA/A$^-$,H$_2$ couple for [NEt$_3$H][BPh$_4$] in CH$_3$CN. This means this system requires a more reducing active species than Co(I) in order to reduce

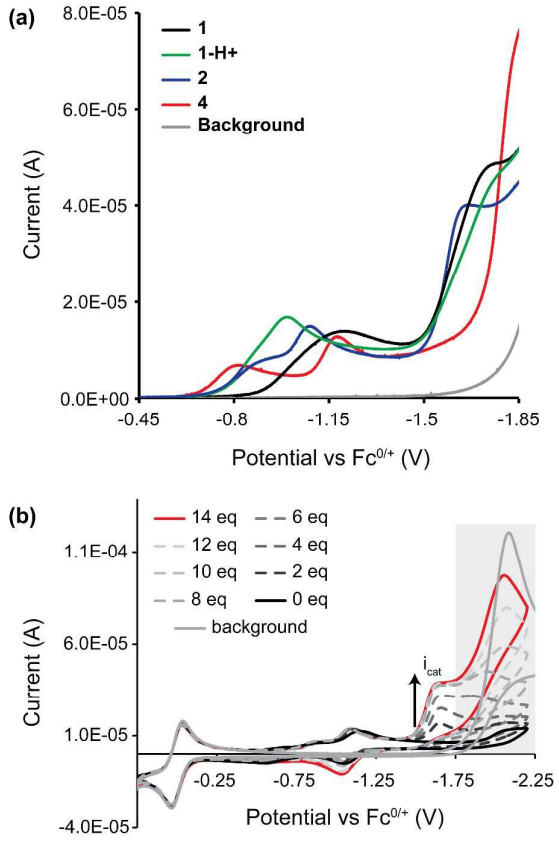


**Figure 4.** (a) Electrocatalytic proton reduction for 0.75mM **1**, **1-H$^+$**, **2** and **4**. At this scan rate, the current reaches limiting conditions at 8 eq of acid. Conditions: 7.5mM [NEt$_3$H][BPh$_4$], 0.2 M [$^n$Bu$_4$N][PF$_6$] in CH$_3$CN at 50 mV/s scan rate (b) Electrocatalytic H$_2$ production for 0.75 mM **2** Conditions: 0-10.5 mM [NEt$_3$H][BPh$_4$], 0.2 M [$^n$Bu$_4$N ][PF$_6$] in CH$_3$CN at 50 mV/s scan rate. For A and B the background scan is with 8 or 14 eq of acid, respectively, in the absence of added catalyst.

[NEt$_3$H][BPh$_4$] to H$_2$.[32] This phenomenon has been observed previously for related cobalt-based electrocatalysts.[8, 33] At 60 equivalents of [NEt$_3$H][BPh$_4$] (Figure S26), the scan rate dependence on the plateau catalytic current was investigated. For Complexes **1** and **4** a plateau current was observed at scan rates above 3 V/s (Figure S27-S28). Complexes **2** and **1-H$^+$** did not reach limiting currents, and therefore rates were not calculated. Under these pseudo first order conditions, we utilized equation 1 to obtain rates for proton reduction (Table 1).[34]

$$i_{cat} = nFAC_p^0\sqrt{D'k_{obs}} \qquad (1)^{35}$$

The rates presented here compare favorably with other cobalt catalysts. Complex **4** affords an $i_{cat}/i_p$ of ~5 at 100 mV/s[23], which can be compared to other complexes that catalyze proton reduction in CH$_3$CN,[16, 28, 36] though these complexes have lower rates than some diglyoxime

counterparts (i.e. - Co[(dmgBF$_2$)$_2$(MeCN)$_2$ $i_{cat}/i_p$ ~40 at 100 mV/s)[12]. All complexes have distinct rates, with the highest observed for Complex **4**.

The overpotentials for Complexes **1**, **1-H$^+$**, **2** and **4** were determined according to the $E_{cat/2}$[9] at 10 eq [NEt$_3$H][BPh$_4$] at a scan rate of 50 mV/s (Table 1). Of interest are the differing overpotentials of **1** and **1-H$^+$**, suggesting that **1** is not completely protonated during electrocatalysis with [NEt$_3$H][BPh$_4$], consistent with our measured p$K_a$ of **1-H$^+$** in CH$_3$CN. The lowest overpotential was found for **2** (320 mV) and the highest was found for **4** (480 mV).

**Table 1.** Overpotentials, first order rate constants ($s^{-1}$), and Faradaic efficiencies for proton reduction listed for Complexes **1**, **1-H$^+$**, **2** and **4** using [NEt$_3$H][BPh$_4$], as an acid source. Rate constants were calculated from $i_{cat}$[35] using 45 mM [NEt$_3$H][BPh$_4$], and 0.75 mM [cat] at 3 V/s (Figure S27-S28), with diffusion coefficients calculated from $^1$H DOSY NMR spectroscopy (Table S2). Faradaic efficiencies were computed from hydrogen measured by GC-TCD following bulk electrolysis using a graphite rod as the working electrode.

| | **1** | **1-H$^+$** | **2** | **4** |
|---|---|---|---|---|
| $k_{obs}$ ( $s^{-1}$) | 46 | | | 170 |
| Overpotential (V) | 0.36 | 0.38 | 0.32 | 0.48 |
| Faradaic Efficiency (%) | 63 | 72 | 21 | 80 |

In order to determine whether the identity of the bound metal would prevent protonation of the O-O binding pocket under electrocatalytic conditions, a stronger acid, [HIm$^{Me}$][BPh$_4$], was investigated as a proton source (Figure S29 and S30). For complexes **1**, **1-H$^+$** and **2**, the onset of catalytic current and molecular reductions prior to the catalytic peak occur at the same potential, suggesting the same catalytically active species. Complex **4,** however, retains distinct molecular peaks, suggesting an increase in acid stability. This suggests that protonation of the O-O binding pocket can be prevented through appropriate choice of the bound cation.

Bulk electrolysis experiments confirm hydrogen production for all catalysts (Table S3-S4 and Figure S31-S36). Experiments were run using 0.25 mM catalyst and 25 mM [NEt$_3$H][BPh$_4$], and $H_2$ was measured using a gas chromatograph equipped with a thermal conductivity detector. Each catalyst was held at its overpotential value for the controlled potential electrolysis. Background proton reduction from the electrode in the presence of acid was determined in each case and subtracted from the total amount of hydrogen produced in the presence of catalyst in order to calculate the reported Faradaic efficiencies provided in Table 1. However, at potentials necessary to observe hydrogen production, a catalytically active film forms during the course of the bulk electrolyses[37-42]. This can be easily visualized using an FTO working electrode (Figure S36) and was confirmed to be a complication in the bulk electrolysis experiments using graphite as shown by the rinsed electrode traces in Figures S31-S34.

## Conclusions

The presented work has demonstrated that the ethylene bridged diimine monoxime monoximate cobalt complex can be cleanly deprotonated and the resulting complex can function as a metalloligand to create a family of multimetallic proton reduction catalysts. These complexes are stable to dissociation at low concentrations in CH$_3$CN and the acid stability of the complexes can be controlled by the identity of the bound cation. The coordination of the doubly deprotonated metalloligand (**1**) with a proton or metal complex results in a shift of Co(III/II) and Co(II/I) to more positive potentials, with overlapping Co(III/II) and (II/I) waves observed for **3** and **1-H$^+$**. While these complexes appear stable under typical catalytic conditions using cyclic voltammetry, they decompose under extended electrolysis conditions resulting in catalytically active films.

## Experimental Section

**General Considerations.**

(DO)(DOH)enCoBr$_2$[20], [NEt$_3$H][BPh$_4$][43] ([$^{Me}$ImH][BPh$_4$] was synthesized analogously; both were recrystallized once from acetone), [HDMF][OTf][44] and RuCl$_2$(bpy)$_2$[45] were synthesized according to published procedures. The phosphazene acid, [2-NO$_2$-4-CF$_3$-C$_6$H$_3$P$_1$H(pyrr)][PF$_6$], was synthesized by Prof. Caroline Saouma from published procedures.[21] NMR solvents were purchased from Cambridge Isotope Labs and used as received. Neat phosphoric and trifluroracetic acid were used as internal standards for $^{31}$P and $^{19}$F NMR experiments, respectively. $^1$H NMR is reported referenced to internal proteo solvent resonances. All other reagents and solvents not highlighted below were bought from Sigma Aldrich and used as received. UV-Vis spectra were acquired on a Cary 5000 spectrophotometer from Agilent Technologies.

The electrolyte [$^n$Bu$_4$N][PF$_6$] used in cyclic voltammetry experiments was either recrystallized two times in EtOH and dried overnight under vacuum at 100 °C or electrochemical grade ≥ 99% was purchased from Sigma-Aldrich. All CV experiments were taken in a $N_2$ filled glove box. Glassy carbon working electrodes (CH Instruments and BASi), platinum auxiliary electrode (BASi) and a Ag wire pseudo reference electrode in a Vycor-fritted compartment (BASi) filled with [$^n$Bu$_4$N][PF$_6$] and CH$_3$CN were used. Glassy carbon electrodes with a diameter of 3.0 mm were polished using 0.05, 0.3 and 1.0 micron polishing powder (CHI instruments) followed by 5 minute sonication cycles in deionized water after every CV that was run for electrocatalytic experiments. All experiments were referenced to an internal ferrocene standard added after the experiment unless otherwise noted, Ultra-high purity acetonitrile used in cyclic voltammetry (Burdick and Johnson) was dried over alumina overnight, subjected to 3 freeze pump thaw cycles, brought in the glove box, filtered and stored over 3 Å molecular sieves. For bulk electrolysis experiments a custom cell was constructed using a curly platinum wire as the auxiliary electrode, a silver wire as the reference electrode, and a graphite rod (Pine Instruments) as the working

electrode. For visualizing catalyst decomposition, FTO-coated glass slides were used as the working electrode. In all cases the cell potential was referenced to ferrocene as an internal standard. Hydrogen was detected using a SRI gas chromatograph equipped with a TCD detector using argon carrier gas and a 6' MS-13X column. Hydrogen was quantified using a calibration curve created by injecting a known amount of hydrogen into the bulk electrolysis cell (Figure S37) and allowing the cell to equilibrate for 10 min with stirring. Aliquots from the headspace of these cells were injected into the GC and the peak for hydrogen was integrated. Rinse test traces were performed by rinsing the used electrode from the given experiment and then using this same electrode in a new solution of the same acid concentration at the same scan rate and potential.

*Caution! Perchlorate salts of metal complexes with organic ligands are potentially explosive and should only be handled in small quantities when in dry form.*

**Synthesis of Complex 1, $[(DO)_2enCo(Im^{Me})_2][ClO_4]$.**

3.438 g (7.74 mmol, 1 eq) of (DOH)(DO)enCo$Br_2$ was suspended in 250 mL of $CH_3CN$. To this solution, 3.06 mL (38.7 mmol, 5 eq) of 1-methyl imidazole was added. The solution became dark red and homogeneous. To this solution 2.884 g (7.74 mmol, 1 eq) of zinc perchlorate hydrate was added. The reaction was stirred overnight and a golden solid crashed out of solution during that time. The reaction mixture was filtered and the solids were washed with acetonitrile. The isolated solids were recrystallized from MeOH. Yield = 2.611 g (4.77 mmol, 63%).

$^1$H NMR (300 MHz, DMSO-$d_6$) 1.87 (6H, s), 2.36 (6H, s), 3.60 (6H, s), 4.66 (4H, s), 6.71 (2H, s), 7.07 (2H, s), 7.52 (2H, s) ppm

$^1$H NMR (499 mHz, $CD_3CN$) 1.93 (6H, s), 2.34 (6H, s), 3.57 (6H, s), 4.55 (4H, s), 6.63 (2H, t), 6.83 (2H, t), 7.28 (2H, s) ppm

$^{13}$C NMR (75 MHz, DMSO-$d_6$) 12.6, 16.9, 34.4, 51.9, 122.1, 127.0, 137.9, 150.4, 176.3 ppm

ε (L mol$^{-1}$ cm$^{-1}$)= 25,000 +/- 240 at 263 nm, ε= 1,800 +/- 120 at 300 nm, ε= 5,000 +/- 60 at 345 nm, ε= 3,000 +/- 20 at 408 nm, ε= 1,700 +/- 30 at 468 nm

Elemental Analysis Calculated for **1** ($C_{18}H_{28}ClCoN_8O_6$): C, 39.53; H, 5.16; N, 20.49. Found: C, 39.47; H, 4.75; N, 20.24.

**Synthesis of Complex 1-H$^+$, $[(DOH)(DO)enCo(Im^{Me})_2][PF_6]_2$.**

0.682 g (1.25 mmol, 1 eq.) of **1** was suspended in 75 mL of $CH_3CN$. To this suspension 0.278 g (1.25 mmol, 1 eq) of [HDMF][OTf] was added. The solution became light yellow and homogeneous on stirring. The $CH_3CN$ was removed by vacuum and the remaining residue was dissolved in water. To this solution, an aqueous solution of excess $[NH_4][PF_6]$ was added and the solid product began to crystallize from solution. After cooling to 3 °C, the solid was filtered and washed with water. Yield = 0.756 g (1.02 mmol, 82%). Alternatively, this complex can by protonated by $CF_3COOH$ and recrystallized from warm MeOH containing excess $NaClO_4$ (yields the perchlorate salt).

$^1$H NMR (500 MHz, $CD_3CN$) 2.32(6H, s), 2.52(6 H, s), 3.63(6H, s), 4.79(4H, s), 5.57(1H, br), 6.51(2H, t), 7.01(2H, st), 7.20(2H, t) ppm

$^{13}$C NMR (125.7 MHz, $CD_3CN$) 14.1, 19.6, 35.8, 55.0, 124.3, 127.0, 139.2, 162.0, 181.1 ppm

$^{19}$F NMR (282.4 MHz, $CD_3CN$) -68.52 (d) ppm; $^1J_{F\text{-}P}$ 705.5 Hz

$^{31}$P NMR (202.4 MHz, $CD_3CN$) -143.15 (sep) ppm; $^1J_{P\text{-}F}$ 707.2 Hz

Elemental Analysis Calculated for **1-H$^+$** ($C_{18}H_{29}CoF_{12}N_8O_2P_2$): C, 29.28; H, 3.96; N, 15.18. Found: C, 29.52; H, 3.83 ;N, 15.01.

**Synthesis of Complex 2, $(DO)_2enCo(Im^{Me})_2ClO_4ZnBr_2$.**

0.117 g (0.21 mmol, 1eq) of **1** and 0.043 g (0.19 mmol, 1 eq) of $ZnBr_2$ were suspended in 5 mL of MeOH and stirred overnight. A light yellow precipitate formed and was isolated by filtration and dried under vacuum. These solids were recrystallized from acetonitrile. Yield = 0.078 g (0.101 mmol, 47%).

$^1$H NMR (499 MHz, DMSO-$d_6$) 2.01 (6H, s), 2.45 (6H, s), 3.60 (6H, s), 4.66 (4H, s), 6.68 (2H, s), 7.14 (2H, s), 7.53 (2H, s) ppm

$^1$H NMR (499 mHz, $CD_3CN$) 2.26 (6H, s), 2.51 (6H, s), 3.64 (6H, s), 4.58 (4H, s), 6.57 (2H, s), 6.99 (2H, s), 7.39 (2H, s) ppm

$^{13}$C NMR (126MHz, $CD_3CN$) 14.21, 19.40, 35.81, 54.53, 123.94, 127.44, 140.40, 161.46, 181.20 ppm

ε (L mol$^{-1}$ cm$^{-1}$)= 11,000 +/- 500 at 292 nm, ε= 1,700 +/- 290 at 397 nm

Elemental Analysis Calculated for **2** ($C_{18}H_{28}Br_2ClCoN_8O_6Zn$): C, 28.00; H, 3.66; N, 14.51. Found: C, 27.63; H, 3.67; N, 14.17.

**Synthesis of Complex 3-Zn, $[(DO)_2enCo(Im^{Me})_2ClO_4]_3Zn(ClO_4)_2$.**

0.150g (0.92 mmol, 3 eq) of **1** was suspended in 50 mL of a 1:1 MeOH:$H_2O$ mixture along with 0.114 g (0.31 mmol, 1 eq) of $Zn(ClO_4)_2$•$6H_2O$ and stirred overnight. Upon evaporation of MeOH and cooling of the solution to 3 °C, a yellow solid crashed out. The supernatant was decanted and the solids were dried under vacuum to yield a yellow-orange powder. Crystals were grown from a 1:1 $H_2O$:MeOH solution. Yield = 0.428 g (0.22 mmol, 73%).

$^1$H NMR (499 mHz, $CD_3CN$) 2.23 (18H, s), 2.50 (18H, s), 3.46 (18H, s), 4.64 (12H, s), 6.68 (6H, s), 6.80 (6H, s), 7.32 (6H, s) ppm

$^{13}$C NMR (126MHz, $CD_3CN$) 13.81, 19.00, 35.58, 54.07, 123.54, 127.89, 139.32, 159.71, 180.61 ppm

ε (L mol$^{-1}$ cm$^{-1}$) = 33,000 +/- 1,000 at 296 nm, ε = 5,700 +/- 300 at 392 nm, ε = 2,000 +/- 100 at 465 nm

Elemental Analysis Calculated for **3-Zn·5$H_2O$** ($C_{54}H_{96}Cl_5Co_3N_{24}O_{32}Zn$): C, 32.22; H, 4.81; N, 16.70. Found: C, 32.63; H, 4.58; N, 16.73.

**Synthesis of Complex 3-Mn, $[(DO)_2enCo(Im^{Me})_2ClO_4]_3Mn(ClO_4)_2$.**

0.080 g (0.15 mmol, 3 eq) of **1** and 0.014 g (0.049 mmol, 1 eq) of $Mn(ClO_4)_2$•$6H_2O$ were suspended in 50 mL of a 1:1 MeOH:$H_2O$ mixture and stirred overnight. The mixture was then decanted and the solids were dried under vacuum. The solids collected were recrystallized from a 1:1 MeOH and $H_2O$ mixture by slow cooling from a 60 °C solution to room temperature overnight. The crystallized solids were collected

and dried under vacuum giving a 50% yield (0.048 g, 0.025 mmol).

ε (L $mol^{-1}$ $cm^{-1}$)= 44,000 +/- 2,700 at 300 nm, ε = 7,700 +/- 300 at 401 nm, ε = 3,100 +/- 240 at 461 nm

Elemental Analysis Calculated for **3-Mn·5$H_2O$** ($C_{54}H_{96}Cl_5Co_3N_{24}O_{32}Mn$): C, 32.39; H, 4.83; N, 16.79. Found: C, 32.89; H, 4.58; N, 16.77.

**Synthesis of Complex 3-Cd, $[(DO)_2enCo(Im^{Me})_2ClO_4]_3Cd(ClO_4)_2$.**

This complex was synthesized using the same prep as **3-Mn**, using 0.311 g (0.57 mmol, 3 eq) of **1** and 0.062 g (0.19 mmol, 1 eq) of $Cd(ClO_4)_2$•$6H_2O$. The product was collected with a 42% yield (0.155 g, 0.079 mmol).

$^1$H NMR (499 mHz, $CD_3CN$) 2.23 (18H, s), 2.47 (18H, s), 3.26 (18H, s), 4.54 (12H, broad s), 4.78 (12H, broad s), 6.53 (6H, s), 6.80 (6H, s), 7.35 (6H, s) ppm

$^{13}$C NMR (126 MHz, $CD_3CN$) 13.69, 18.88, 35.34, 53.73, 122.89, 128.51, 139.27, 159.10, 180.47 ppm

ε (L $mol^{-1}$ $cm^{-1}$) = 68,000 +/- 1,500 at 259 nm, ε = 40,000 +/- 670 at 297 nm, ε = 7,000 +/- 450 at 404 nm

Elemental Analysis Calculated for **3-Cd·5$H_2O$** ($C_{54}H_{96}Cl_5Co_3N_{24}O_{32}Cd$): C, 31.49; H, 4.70; N, 16.32. Found: C, 31.82; H, 4.47; N, 16.35.

**Synthesis of Complex 4, $(DO)_2enCo(Im^{Me})_2Ru(bpy)_2(OTf)_3$.**

0.500 g (1.03 mmol, 1 eq) of $RuCl_2(bpy)_2$ was suspended in 20 mL of a 2:1 EtOH:$H_2O$ mixture. To this suspension, 0.531 g (2.06 mmol, 1 eq) of AgOTf was added and the mixture was stirred for 30 min at 60 °C. This solution was filtered through Celite to remove AgCl and the solvent was then removed under vacuum. To this red solid, 4 mL of 2:1 ethanol:water was added. 0.565 g (1.03 mmol, 1 eq) of **1** was added and the reaction mixture was stirred overnight at 60 °C (refluxing the reaction or heating to higher temperatures will favor the formation of $Ru(bpy)_2(Im^{Me})_2(OTf)_2$). The solvent was again evaporated and the resulting purple solid was suspended in 4-6 mL of $H_2O$. This suspension was filtered and washed sparingly with water. Yield= 0.467 g (0.40 mmol, 38.5%). The $ClO_4$ anion was exchanged for OTf by dissolving the product in water (~250 mL for 0.5 g), adding an aqueous solution of excess LiOTf, and cooling to 3 °C. From this solution a fine powder crystallizes.

$^1$H NMR (499 mHz, $CD_3CN$) 2.20 (18H, s), 2.48 (18H, s), 3.44 (18H, s), 3.79 (12H, d), 4.23 (12H, d), 5.97 (6H, s), 6.54 (6H, s), 6.85 (6H, s), 7.18-7.21 (4H, m), 7.57 (2H, d), 7.86 (2H, t), 7.99-8.03 (4H, m), 8.36 (2H, d), 8.43 (2H, d) ppm

$^{13}$C NMR (499MHz, $CD_3CN$) 14.40, 19.21, 36.01, 54.55, 120.85, 123.41. 124.11, 124.34, 124.62, 126.41, 126.76, 137.10, 138.90, 151.53, 154.30, 159.28, 160.96, 161.75, 179.00 ppm

$^{19}$F NMR (499MHz, $CD_3CN$) -77.25 ppm

ε (L $mol^{-1}$ $cm^{-1}$) = 70,000 +/- 1,000 at 295 nm, ε= 11,000 +/- 28 at 373 nm, ε= 10,000 +/- 50 at 420 nm, ε= 19,000 +/- 300 at 502 nm

Elemental Analysis Calculated for **4** ($C_{42}H_{48}CoF_9N_{12}O_{11}RuS_3$): C, 38.10; H, 3.65; N, 12.69. Found: (average of 3 trials of 2 separate syntheses with standard deviation) C, 35.52 ± 0.389; H, 3.62 ± 0.14; N, 12.11 ± 0.18.

## Acknowledgements

This research was supported by startup funds from the University of Washington and the ACS Petroleum Research Fund through grant number 54226-DNI3.

## Notes and references

Abbreviations used in the text: DO = dioximate, en = ethylene backbone ($RCH_2CH_2R$), $Im^{Me}$ = 1-methylimidazole.

1. Ceccon, A.; Santi, S.; Orian, L.; Bisello, A., *Coord. Chem. Rev.* **2004,** *248*, 683-724.
2. Wheatley, N.; Kalck, P., *Chem. Rev.* **1999,** *99*, 3379-3420.
3. Stephan, D. W., *Coord. Chem. Rev.* **1989,** *95*, 41-107.
4. van den Beuken, E. K.; Feringa, B. L., *Tetrahedron* **1998,** *54*, 12985-13011.
5. Berben, L.; Peters, J., *Chem. Commun.* **2009,** *46*, 398-400.
6. McCrory, C.; Uyeda, C.; Peters, J., *J. Am. Chem. Soc.* **2012,** *134*, 3164-3170.
7. Jacques, P.-A.; Artero, V.; Pecaut, J.; Fontecave, M., *Proc. Natl. Acad. Sci.* **2009,** *106*, 20627-20632.
8. Razavet, M.; Artero, V.; Fontecave, M., *Inorg. Chem.* **2005,** *44*, 4786-4795.
9. Fourmond, V.; Jacques, P.-A.; Fontecave, M.; Artero, V., *Inorg. Chem.* **2010,** *49*, 10338-10347.
10. Baffert, C.; Artero, V.; Fontecave, M., *Inorg. Chem.* **2007,** *46*, 1817-1824.
11. Hu, X.; Cossairt, B. M.; Brunschwig, B. S.; Lewis, N. S.; Peters, J. C., *Chem. Commun.* **2005**, 4723-4725.
12. Hu, X.; Brunschwig, B. S.; Peters, J. C., *J. Am. Chem. Soc.* **2007,** *129*, 8988-8998.
13. Connolly, P.; Espenson, J. H., *Inorg. Chem.* **1986,** *25*, 2684-2688.
14. Chao, T.-H.; Espenson, J. H., *J. Am. Chem. Soc.* **1978,** *100*, 129-133.
15. Valdez, C. N.; Dempsey, J. L.; Brunschwig, B. S.; Winkler, J. R.; Gray, H. B., *Proc. Natl. Acad. Sci.* **2012,** *109*, 15589-15593, S15589/1-S15589/3.
16. Kelley, P.; Radlauer, M.; Yanez, A.; Day, M.; Agapie, T., *Dalton Trans.* **2012,** *41*, 8086-8.
17. Uyeda, C.; Peters, J. C., *Chem. Sci.* **2013,** *4*, 157-163.
18. Uyeda, C.; Peters, J. C., *J. Am. Chem. Soc.* **2013,** *135*, 12023-12031.
19. Birkelbach, F.; Winter, M.; Floerke, U.; Haupt, H.-J.; Butzlaff, C.; Lengen, M.; Bill, E.; Trautwein, A.; Wieghardt, K.; Chaudhuri, P., *Inorg. Chem.* **1994,** *33*, 3990-4001.
20. Kitiphaisalnont, P.; Thohinung, S.; Hanmungtum, P.; Chaichit, N.; Patrarakorn, S.; Siripaisarnpipat, S., *Polyhedron* **2006,** *25*, 2710-2716.
21. Kaljurand, I.; Kütt, A.; Sooväli, L.; Rodima, T.; Mäemets, V.; Leito, I.; Koppel, I. A., *J. Org. Chem.* **2005,** *70*, 1019-1028.
22. Soloviev, V.; Eichhöfer, A.; Fenske, D.; Banin, U., *J. Am. Chem. Soc.* **2001,** *123*, 2354-2364.
23. Rose, M. J.; Gray, H. B.; Winkler, J. R., *J. Am. Chem. Soc.* **2012,** *134*, 8310-8313.
24. Savéant, J.-M., *Elements of molecular and biomolecular electrochemistry*. John Wiley and Sons Inc.: Hoboken, New Jersey, 2006.

25. Bard, A. J.; Faulkner, L. R., *Electrochemical Methods Fundamentals and Applications*. 2nd ed.; Wiley: Hoboken, NJ, 2001.
26. Kolthoff, I. M.; Chantooni, M. K.; Bhowmik, S., *Anal. Chem.* **1967,** *39*, 1627-1633.
27. Izutsu, K., *Acid-Base Dissociation Constants in Dipolar Aprotic Solvents; IUPAC Chemical Data Series*. Blackwell Science: Oxford, UK, 1990.
28. Ahn, H. S.; Davenport, T. C.; Tilley, T. D., *Chem. Commun.* **2014,** *50*, 3834-3837.
29. Artero, V.; Fontecave, M., *Chem. Soc. Rev.* **2013,** *42*, 2338-2356.
30. Dempsey, J. L.; Brunschwig, B. S.; Winkler, J. R.; Gray, H. B., *Acc. Chem. Res.* **2009,** *42*, 1995-2004.
31. Marinescu, S. C.; Winkler, J. R.; Gray, H. B., *Proc. Natl. Acad. Sci.* **2012,** *109*, 15127-15131.
32. Felton, G. A. N.; Glass, R. S.; Lichtenberger, D. L.; Evans, D. H., *Inorg. Chem.* **2006,** *45*, 9181-9184.
33. Wiedner, E. S.; Appel, A. M.; DuBois, D. L.; Bullock, R. M., *Inorg. Chem.* **2013,** *52*, 14391-14403.
34. Andrieux, C. P.; Blocman, C.; Dumas-Bouchiat, J. M.; M'Halla, F.; Savéant, J. M., *J. Electroanal. Chem. Interfacial. Electrochem.* **1980,** *113*, 19-40.
35. In equation 1, $i_{cat}$ = catalytic current (A), n = number of electrons consumed in the catalytic cycle (2), A = area of the electrode ($cm^2$), $C_p^0$ = concentration of the catalyst ($mol/cm^3$), D = diffusion coefficient ($cm^2/s$), and $K_{obs}$ = observed rate constant ($s^{-1}$).
36. Kal, S.; Filatov, A. S.; Dinolfo, P. H., *Inorg. Chem.* **2014,** *53*, 7137-7145.
37. Williams, O. M.; Cowley, A. H.; Rose, M. J., *Dalton Trans.* **2015,** *DOI: 10.1039/C5DT00924C*.
38. Anxolabéhère-Mallart, E.; Costentin, C.; Fournier, M.; Nowak, S.; Robert, M.; Savéant, J.-M., *J. Am. Chem. Soc.* **2012**, 6104-6107.
39. El Ghachtouli, S.; Fournier, M.; Cherdo, S.; Guillot, R.; Charlot, M.-F.; Anxolabéhère-Mallart, E.; Robert, M.; Aukauloo, A., *J. Phys. Chem. C* **2013,** *117*, 17073-17077.
40. El Ghachtouli, S.; Guillot, R.; Brisset, F.; Aukauloo, A., *ChemSusChem* **2013,** *6*, 2226-2230.
41. Anxolabéhère-Mallart, E.; Costentin, C.; Fournier, M.; Robert, M., *J. Phys. Chem. C* **2014,** *118*, 13377-13381.
42. McCarthy, B. D.; Donley, C. L.; Dempsey, J. L., *Chem. Sci.* **2015,** *6*, 2827-2834.
43. Casely, I. J.; Ziller, J. W.; Mincher, B. J.; Evans, W. J., *Inorg. Chem.* **2010,** *50*, 1513-1520.
44. Favier, I.; Duñach, E., *Tetrahedron Lett.* **2004,** *45*, 3393-3395.
45. Norris, M. R.; Concepcion, J. J.; Glasson, C. R. K.; Fang, Z.; Lapides, A. M.; Ashford, D. L.; Templeton, J. L.; Meyer, T. J., *Inorg. Chem.* **2013,** *52*, 12492-12501.